Superconducting Properties of Metastable bcc Solid Solution in Melt-quenched Zr-Ge Binary Alloys

Superconducting Properties of Metastable bcc Solid Solution in Melt-quenched Zr-Ge Binary Alloys*

Akihisa Inoue, Yoshimi Takahashi**, Shigeki Okamoto***,
Tsuyoshi Masumoto and H. S. Chen****
The Research Institute for Iron, Steel and Other Metals

(Received December 16, 1982)

Synopsis

Superconducting metastable bcc phase has been found in rapidly quenched Zr-Ge binary alloys in a composition range 9 to 12 at% Ge. With decreasing germanium content, the T_c value of the bcc alloys increased from 3.30 to 3.88 K,while the H_{c2} gradient at T_c,$-(dH_{c2}/dT)_{T_c}$, and the electrical resistivity at 4.2 K, ρ_n, decreased from 1.86×10^6 to 1.79×10^6 Am^{-1} K^{-1} and 2.00 to 1.70 $\mu\Omega m$, respectively. There existed a strong correlation between ρ_n, T_c and $-(dH_{c2}/dT)_{T_c}$; with increasing ρ_n, T_c decreased and $-(dH_{c2}/dT)_{T_c}$ increased. A correlation between the temperature coefficient of resistivity (TCR), $1/\rho_{R.T.}(d\rho/dT)$ and T_c was also found; the larger the TCR the higher is the T_c. The existence of such correlations was inferred to originate from the close relation between the electron-phonon coupling constant λ and ρ_n or TCR. The electronic dressed density of states at the Fermi level $N(E_f)(1+\lambda)$ was calculated from the experimentally measured values of $-(dH_{c2}/dT)_{T_c}$ and ρ_n by using theories for strong-coupling superconductors. It was found that the values of $N(E_f)(1+\lambda)$ significantly reflect T_c. The GL parameter κ and the GL coherence length $\xi_{GL}(0)$ were estimated to be 69-79 and about 7.5 nm, respectively, from the experimental values of $-(dH_{c2}/dT)_{T_c}$ and ρ_n. The metastable bcc Zr-Ge alloys are concluded to be extremely "dirty" type-II superconductors.

I. Introduction

---

* The 1759th report of the Research Institute for Iron, Steel and Other Metals.

** Permanent address, Sonny Magnet Products, Tagajo 985, Japan.

*** Graduate School, Tohoku University, Sendai 980, Japan.

**** Bell Laboratories, 600 Mountain Avenue, Murray Hill, New Jersey 07974, U.S.A.

For the past few years, numerous studies on the superconducting properties of melt-quenched amorphous alloys have emerged [1-3]. It has been found that an amorphous superconductor exhibits unique characteristics which are not observed in crystalline counterparts. The main characteristics are summarized in the following.

(i) A sharp transition to the superconducting state from extremely high electrical resistivities ($\rho_n > 1.0 \mu\Omega m$).

(ii) The appearance of large flux flow resistivity $\rho_f(H)$ and extremely low critical current density $J_c(H)$ as a result of a homogeneous structure on the scale of coherence length, and consequently of very weak flux pinning force.

(iii) A large temperature dependence of upper critical field.

(iv) High stability of superconducting properties against tensile and bending strains, cold working and neutron irradiation.

Recently, Inoue et al. [4-6] have demonstrated that in melt-quenched Zr-Si binary alloys an amorphous phase forms in the range of 13-24 at% Si and a metastable bcc solid solution in the range of 9-12 at% Si and found that superconducting properties in many features are very similar in these two phases. The similarity in superconducting characteristics of the bcc phase and the amorphous phase, in spite of the distinctly different structure, was attributed to the fact that the bcc solid solution saturated with silicon was in an extremely metastable state containing a high density of internal defects, numerous grain boundaries and high internal strains. The above-mentioned superconducting characteristics of the amorphous alloys and thus the metastable bcc Zr-Si alloys are significantly different from those of crystalline superconductors obtained by conventional fabrication process. Systematic investigations of the superconducting properties of the metastable bcc solid solutions in series of alloy systems quenched from the melts and clarification of these features in comparison with an amorphous superconductor and conventional crystalline superconductors are thus technologically and scientifically important. This paper presents the formation range, hardness, normal electrical resistivity and superconducting properties of the metastable bcc solid solution in melt-quenched Zr-Ge binary alloys.

II. Experimental Procedure

The Zr-Ge alloys were prepared from high purity components by arc melting under a protective argon atmosphere. The alloys were repeatedly remelted to ensure compositional homogeneity. Long and continuous ribbons of about 1 mm width and about 20 μm thickness were

obtained by a modified single roller melt-spinning method in which the alloy is levitation melted [7]. The as-quenched phase of the samples was characterized by X-ray and electron metallographic techniques which have been detailed elsewhere [8]. Hardness (H_V) was measured by a Vickers microhardness tester with a 100 g load. The Young's modulus sound velocity (V_E) along the longitudinal direction of the ribbon samples was measured at 100 kHz using a pulse-echo technique. The measurements of H_V and V_E were conducted at ambient temperatures. Bend ductility testing was done for the as-cast ribbons, and samples which were able to sustain a 180° bending were designated to be ductile. The surface after a 180° bending was observed by a scanning electron microscope. All measurements of superconducting properties T_c and $H_{c2}(T)$ were done resistively using a conventional four probe technique. The temperature was measured with an accuracy of ±0.01 K using a calibrated germanium thermometer. The magnetic field up to 7.2×10^6 A/m was applied perpendiculary to the specimen surface and feed current.

III. Results

1. Formation range and hardness of the metastable bcc phase

Figure 1 shows the composition range in which the bcc solid solution saturated with germanium was found to form without any trace of equilibrium hcp α-Zr and bct Zr_3Ge phases in the Zr-Ge binary systems. In the figure, the data of Zr-Si alloys [5,6] are also presented for comparison. The bcc phase forms in the range of 9 to 12 at% Ge, which is below the concentration for the amorphous phase formation region (13-21 at% Ge). The lattice parameter tends to increase with increasing germanium content, e.g., 0.3715 nm for $Zr_{89}Ge_{11}$ and 0.3733 nm for $Zr_{88}Ge_{12}$. These values are considerably larger than that (0.3609 nm) for pure bcc β-zirconium at a temperature of 1135 K [9], indicating that the bcc phase is a highly supersatu-

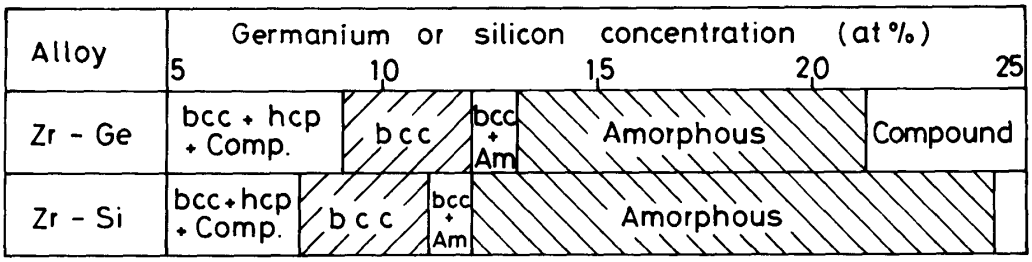

Fig. 1 Composition ranges for the formation of a bcc phase and an amorphous phase in the Zr-Ge system. The data of the Zr-Si system are also shown for comparison.

rated solid solution containing germanium element. Attempt was made to examine, with transmission electron microscopic observation, the internal structure of the bcc phase without fruitful result because of the difficulty in producing a thin foil without contamination. However, considering the microstructure of the metastable bcc phase in melt-quenched Zr-Si alloys [6], it is reasonably inferred that the bcc phase in Zr-Ge system also contains a high density of internal defects, numerous grain boundaries and sub-grain boundaries. It can be seen in Fig. 1 that the formation range of the bcc phase is almost the same between Zr-Ge and Zr-Si systems. The cause for the bcc phase formation in such alloy composition ranges has been presented elsewhere [6].

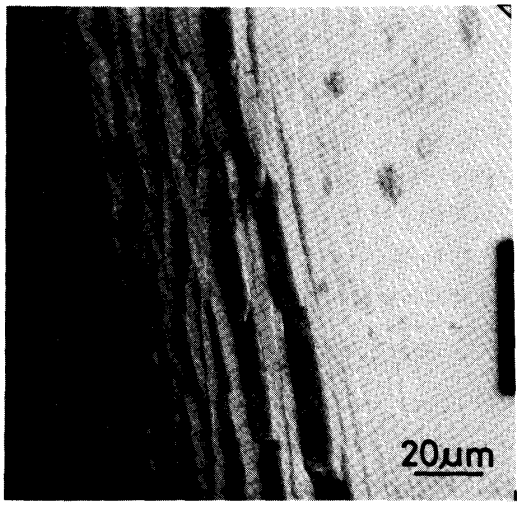

Fig. 2 Scanning electron micrograph showing the deformation marking at the tip of the bcc $Zr_{88}Ge_{12}$ alloy bent through 180°.

It was striking to note that the alloys with a bcc structure of such a high solute content are so ductile that no crack is found at the tip of a specimen bent through 180°, as shown in Fig. 2, as observed in the amorphous phase. Vickers hardness (H_V) and Young's modulus sound velocity ($V_E=\sqrt{E/\rho}$) of the metastable bcc alloys are plotted as a function of germanium content in Figs. 3 and 4, where the data of the amorphous phase are also shown for reference. The H_V and V_E increase from 425 to 496 DPN and from 3.41 to 3.59 km/s, respectively, with increasing germanium content. Such germanium composition dependences of H_V and V_E are similar to those for the amorphous Zr-Ge alloys [10, 11]. The values of H_V and $\sqrt{E/\rho}$ are almost the same level between the bcc and amorphous phases, but one can see a drastic change of hardness and

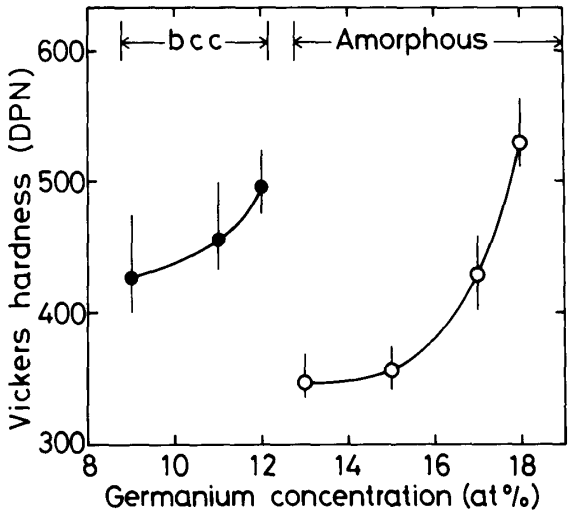

Fig. 3 Germanium composition dependence of the Vickers hardness (H_V) for bcc $Zr_{100-x}Ge_x$ alloys. The data of amorphous Zr-Ge alloys are also shown.

Young's modulus sound velocity upon the structural change of the bcc to amorphous phase in the vicinity of 12-13 at% Ge. This indicates that the difference in long range atomic configuration strongly affects the hardness and Young's modulus. The similar tendency of hardness [6] and Young's modulus sound velocity [11] has been also recognized for Zr-Si alloys in metastable bcc and amorphous phases.

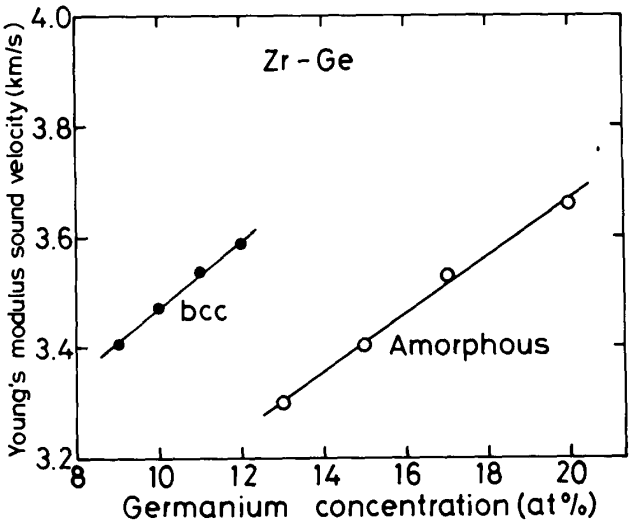

Fig. 4 Germanium composition dependence of the Young's modulus sound velocity (V_E) for bcc and amorphous $Zr_{100-x}Ge_x$ alloys.

2. Electrical Resistivity

The electrical resistivity, ρ_n, at 4.2 K and the temperature coefficient of resistivity (TCR) around room temperature, $1/\rho_{R.T.}(d\rho/dT)$, for the bcc Zr-Ge alloys are presented as a function of germanium content in Fig. 5, along with the data of amorphous Zr-Ge alloys. Although the magnitude of resistivity contains a rather large uncertainty owing to the lack of uniformity in ribbons, it is concluded that the average resistivity monotonically increases with the amount of germanium from 1.70 to 2.00 μΩm for the bcc phase and from 2.35 to 3.10 μΩm for the amorphous phase. Meanwhile, as shown in Fig. 5, the TCR decreased with increasing resistivity and changes a sign from positive, for the bcc alloys except $Zr_{88}Ge_{12}$, to negative for the amorphous phase, passing

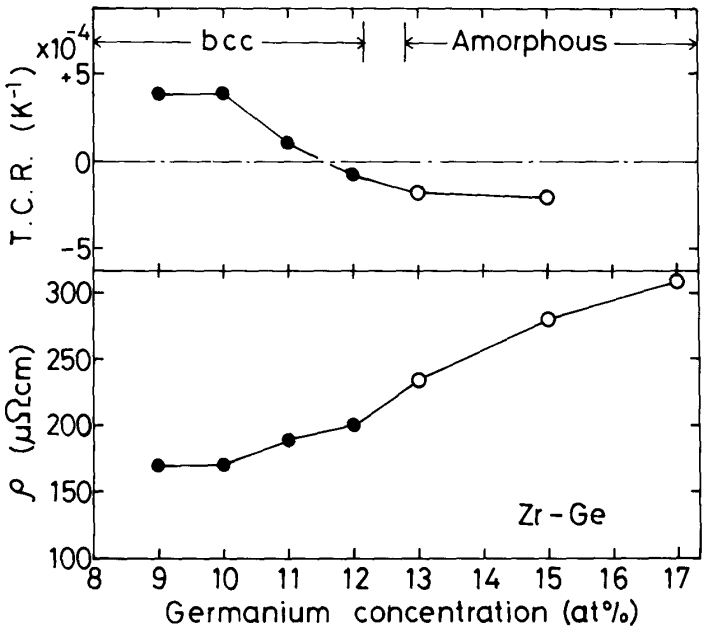

Fig. 5 Germanium concentration dependences of the electrical resistivity ρ_n at 4.2 K and the temperature coefficient of resistivity (TCR) $1/\rho_{R.T.}(d\rho/dT)$ for bcc $Zr_{100-x}Ge_x$ alloys. The data of amorphous Zr-Ge alloys are also shown.

through zero around the resistivity ≃1.70-1.80 μΩm. Such a correlation between ρ_n and TCR is consistent with the general tendency for a large number of crystalline and amorphous alloys [12-14].

3. Superconducting Properties

Figure 6 shows the germanium composition dependences of T_c and the transition width ΔT_c of the bcc Zr-Ge alloys, together with the data of the amorphous Zr-Ge alloys, where T_c is the temperature corresponding to $R/R_n=0.5$. R_n is the resistance in the normal state, and ΔT_c represented by a vertical bar in the figure shows the temperature interval between 0.1 and 0.9 R/R_n. T_c rises from 3.30 to 3.88 K with decreasing germanium content. These values lie on the line extrapolated from the data of the amorphous phase. From the fact that T_c varies monotonically with germanium content without apparent discontinuity at the bcc and amorphous phase boundaries, it is inferred that (1)T_c is closely related to the atomic configurations on the localized scale of atomic distances and there is no apparent change in atomic configuration in atomic scale dimension between the metastable bcc and amorphous phases, and (2) the local atomic ordering of the amorphous alloys resembles that of the metastable bcc phase, but not that of the equilibrium hcp α-Zr phase. Figure 6 also shows that the appearance of hcp α-Zr and an unidentified Zr-Ge compound results in a significant lowering of T_c and the $Zr_{92}Ge_8$ alloy with the mix structure remains in a normal state down to a temperature as low as 2.1 K. The highest T_c value (3.88 K) of the bcc phase is about 6.4 times higher than $T_c=0.61$ K [15] of hcp α-Zr metal. It was also seen that the mixed structure consisting of hcp α- and bcc β- zirconium and an unidentified Zr-Ge compound exhibits a remarkably large ΔT_c as compared with the bcc and amorphous phase. From the variation of T_c with ger-

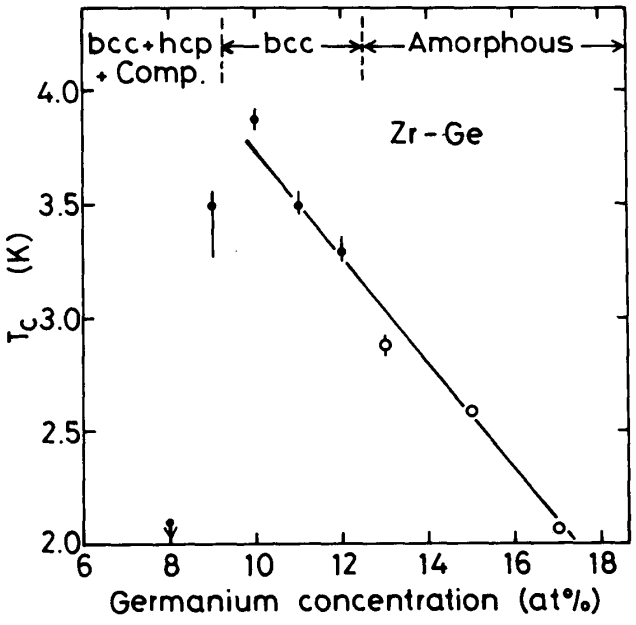

Fig. 6 Germanium composition dependences of the as-quenched structure, the superconducting transition temperature T_c and the transition width ΔT_c for melt-quenched $Zr_{100-x}Ge_x$ alloys. Vertical bars represent the transition width.

manium content, it is expected that a hypothetical bcc pure zirconium would exhibit a T_c value of ≈6.2 K. This extrapolated value is nearly equal to the hypothetical value (≈5.6 K) of "amorphous pure zirconium" predicted from the data of T_c in $Zr_{50-75}Cu_{25-50}$ amorphous alloys [16].

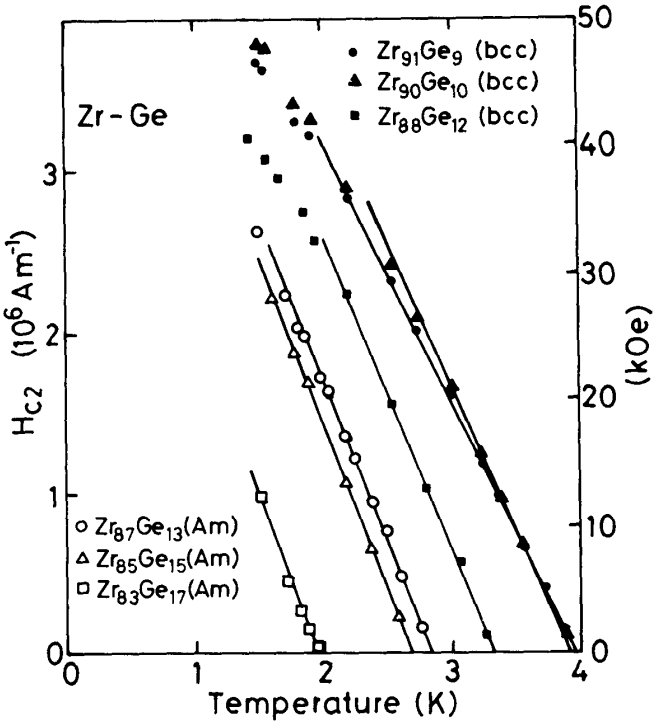

Fig. 7 The upper critical magnetic field H_{c2} at various temperatures for bcc $Zr_{100-x}Ge_x$ alloys. The solid lines represent a linear extapolation at T_c. The data of amorphous Zr-Ge alloys are also represented.

The upper critical magnetic field, H_{c2}, was measured at various temperatures ranging from 1.5 K to T_c. Figure 7 shows the $H_{c2}(T)$ vs temperature (T) plots. Here the H_{c2} was taken as the applied field at which the resistance of the sample begins to deviate from its normal value. Over the temperature range measured, the H_{c2} value is much higher for the bcc phase than for the amorphous phase. This corresponds to the fact that T_c is higher for the former alloys. H_{c2} is seen to increase linearly with decreasing temperature in the temperature range just below T_c and the relation can be expressed as follows.

$$H_{c2}(T) = \left[\frac{dH_{c2}}{dT}\right]_{T_c}(T-T_c) \qquad (1)$$

The gradient at T_c, $-(dH_{c2}/dT)_{T_c}$, is estimated to be 1.65×10^6 $Am^{-1}K^{-1}$ for $Zr_{91}Ge_9$, 1.79×10^6 $Am^{-1}K^{-1}$ for $Zr_{90}Ge_{10}$, 1.82×10^6 $Am^{-1}K^{-1}$ for $Zr_{89}Ge_{11}$ and 1.86×10^6 $Am^{-1}K^{-1}$ for $Zr_{88}Ge_{12}$, being lower than those (1.96×10^6-2.51×10^6 $Am^{-1}K^{-1}$)[10] for the amorphous Zr-Ge alloys. It is important to note that the gradient values at T_c increase with increasing germanium content and/or electrical resistivity.

IV. Discussion

1. Relation between ρ_n and T_c

It has been [17-19] established for some superconducting compounds that there exists a strong correlation between increases in the residual resistivity ρ_n and decreases in the T_c. More recently, Inoue et al. also found the existence of the similar correlation between ρ_n and T_c for some amorphous alloy systems of Zr-Si [5,20], Zr-Ge [10,20], Zr-Nb-Si [21], Zr-Nb-Ge [22] and Mo-Si-B [23]. To investigate the correlation between ρ_n and T_c for the metastable bcc alloys with high resistivities, the experimental values of T_c and $-(dH_{c2}/dT)_{T_c}$ for the bcc Zr-Ge alloys are plotted as a function of electrical resistivity ρ_n at 4.2 K in Fig. 8. The data of amorphous Zr-Ge [10] alloys are also represented for comparison. Although there is a rather large scattering, one can see the tendency that the T_c value decreases and the $-(dH_{c2}/dT)_{T_c}$ value increases with increasing electrical resistivity. The higher T_c values for the bcc alloys appear to be closely related to the lower values of electrical resistivity. Additionally, as shown in Fig. 9, the T_c values of the bcc alloys tend to increase with increasing the magnitude of TCR. This tendency implies that the increase in the temperature dependent part of the resistivity due to phonon scattering results in a rise of T_c. A similar tendency has been recognized for thin films of Nb_3Ge and Nb [17-19] and the origin has been interpreted by the following approximate equation which is applicable in the temperature range of $T>>\theta_D$.

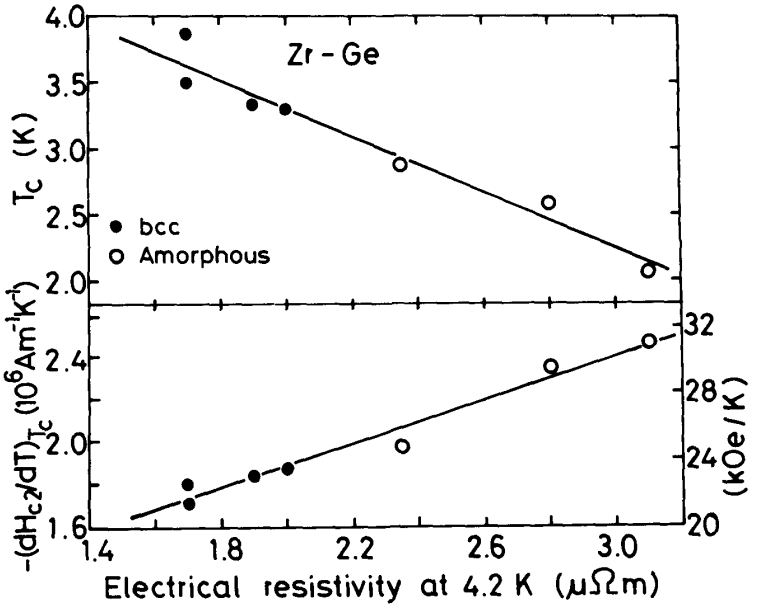

Fig. 8 Correlation between electrical resistivity ρ_n at 4.2 K and T_c or $-(dH_{c2}/dT)_{T_c}$ for bcc $Zr_{100-x}Ge_x$ alloys. The data of amorphous Zr-Ge alloys are also plotted for reference.

$$[\rho(T)-\rho_n]/T = [N(E_f)\langle v_f^2\rangle/3]^{-1}(2\pi k_B/e^2h)\lambda_{tr} \qquad (2)$$

Here $N(E_f)$ is the bare density of states at the Fermi level, v_f is the Fermi velocity and λtr is a coupling constant closely related to λ defined by the function $\alpha^2(\omega)F(\omega)$ in the McMillan theory [25] for the strong-coupling superconductors, which is described in more detail below. If one assumes that the factor $N(E_f)\langle v_f^2\rangle$ remains constant with varying temperature [26], then $d\rho/dT$ in the temperature range $T>>\theta_D$ is essentially proportional to λ. The equation (2) also implies that the increase in ρ_n results in a small λ value. Thus, there is a tendency that the smaller the ρ_n value and the larger the $d\rho/dT$ value, the larger is the λ value. Accordingly, the strong correlation between T_c and ρ_n or TCR appears to originate from the change in λ. Further, the reason why the resistivity of the bcc phase is lower compared with the amorphous phase may be due to the combined effect of the following two factors: (1) the increase in conduction electrons due to the decrease of germanium element exhibiting semiconducting nature, and (2) the decreases of structural disorder and defects which cause the scattering of conduction electrons.

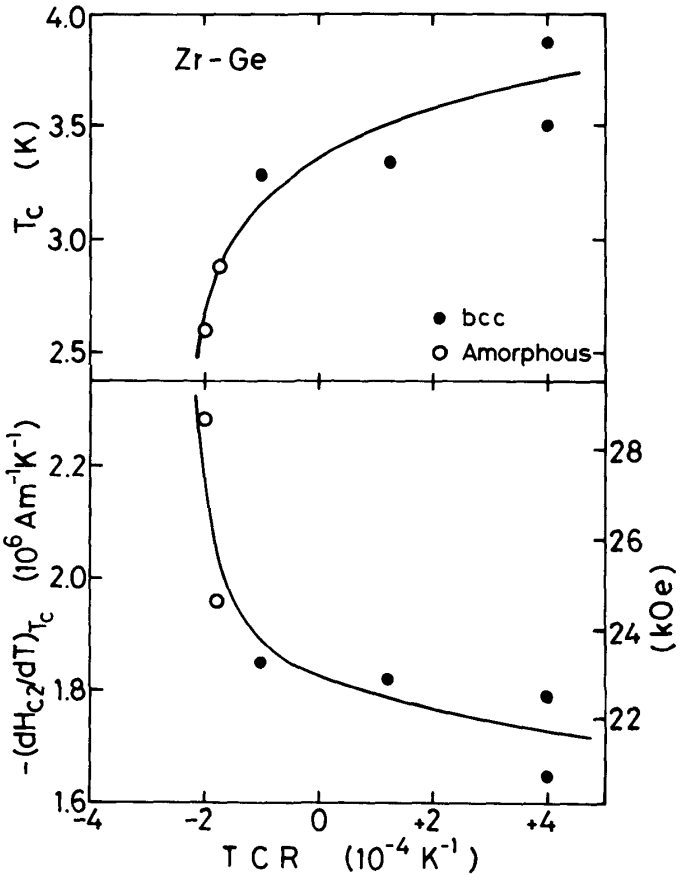

Fig. 9 Correlation between TCR and T_c or $-(dH_{c2}/dT)_{Tc}$ for bcc $Zr_{100-x}Ge_x$ alloys. The data of amorphous Zr-Ge alloys are also plotted for reference.

2. Dominating parameters for T_c

It is well known [25] that the T_c value for a strong coupling superconductor is dominated by the Debye temperature θ_D, λ and/or $N(E_f)$ and the larger the θ_D, λ and $N(E_f)$, the higher is the T_c. In order to examine the reason for the rise of T_c with decreasing germanium content and upon the structural change of amorphous to bcc phase, we estimated the electronic dressed density of states at the Fermi level

$N^*(E_f)=N(E_f)(1+\lambda)$ from the measured values of the H_{c2} gradient at T_c, $-(dH_{c2}/dT)_{T_c}$, and electrical resistivity at 4.2 K, ρ_n, by using the following formulas based on the Ginzburg-Landau-Abrikosov-Gorkov (GLAG) theory [27].

$$N(E_f)(1+\lambda) = -\frac{\pi}{8k_B e\rho_n}\left[\frac{dH_{c2}}{dT}\right]T_c \tag{3}$$

The formula is applicable in the dirty limit where the electron mean free path is much less than the superconducting coherence length $\ell<<\xi$. This criterion is well satisfied for the bcc Zr-Ge alloys since the coherence length is about 7.5 nm as shown later and the mean free path is estimated to be less than 1 nm from the experimental resistivity (1.70-2.00 μΩm) by using the following equations based on the nearly free electron model [28].

$$\ell = \frac{mv_f}{ne^2\rho_n} \tag{4}$$

$$v_f = \frac{\hbar}{m}(3\pi^2 n)^{1/3} \tag{5}$$

Here m and n are the electron mass and the density of electrons per unit volume, respectively. The values of $N(E_f)(1+\lambda)$ thus obtained are summarized in Table 1, together with the values of T_c, ΔT_c, ρ_n

Table 1 Superconducting and the related properties of bcc and amorphous Zr-Ge alloys

Alloy (at%)	T_c (K)	ΔT_c (K)	ρ_n (μΩm)	$-(dH_{c2}/dT)_{T_c}$ ($10^6 Am^{-1}K^{-1}$)	$N(E_f)(1+\lambda)$ (10^{47} states $.m^{-3}.J^{-1}.spin^{-1}$)	$\xi_{GL}(0)$ (nm)	κ	λ_o (nm)	D (mm^2/s)	As-Q structure
$Zr_{91}Ge_9$	3.50	0.48	1.70	1.65	2.17	7.9	66	732	53.0	bcc
$Zr_{90}Ge_{10}$	3.88	0.10	1.70	1.79	2.36	7.2	69	695	48.8	bcc
$Zr_{89}Ge_{11}$	3.34	0.11	1.90	1.82	2.14	7.7	74	792	47.9	bcc
$Zr_{88}Ge_{12}$	3.30	0.10	2.00	1.86	2.07	7.6	76	817	47.1	bcc
$Zr_{87}Ge_{13}$	2.88	0.07	2.35	1.96	1.86	8.0	85	948	44.6	Amorphous
$Zr_{85}Ge_{15}$	2.59	0.05	2.80	2.29	1.82	7.8	101	1092	38.2	Amorphous

and $-(dH_{c2}/dT)_{T_c}$ at T_c. Additionally, the data of the amorphous Zr-Ge alloys are also shown in the table for comparison. The $N(E_f)(1+\lambda)$ values for the bcc Zr-Ge alloys decrease from 2.36×10^{47} to 2.07×10^{47} states $.m^{-3}.J^{-1}.spin^{-1}$ with increasing germanium content. The relation between T_c and $N(E_f)(1+\lambda)$ is shown in Fig. 10 along with the data of amorphous Zr-Ge [10] alloys. It can be seen that the values of $N(E_f)(1+\lambda)$ strongly reflect on T_c: that is, the larger the values of $N(E_f)$ and/or λ, the higher is the T_c. In addition, the $N(E_f)(1+\lambda)$ values of the bcc Zr-Ge alloys are considerably higher than that (2.00×10^{47} states $.m^{-3}.J^{-1}.spin^{-1}$) [15] of hcp α-zirconium metal. This appears to be one of the reasons why the bcc alloys exhibit higher T_c values compared with hcp zirconium metal.

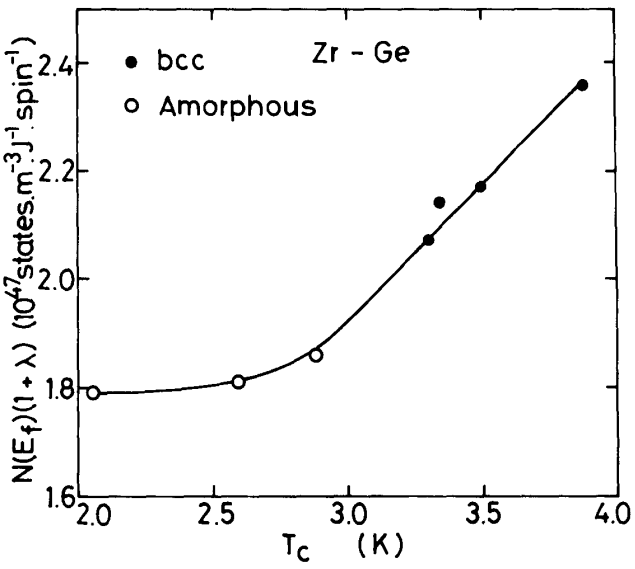

Fig. 10 Correlation between T_c and $N(E_f)(1+\lambda)$ for bcc $Zr_{100-x}Ge_x$ alloys. The data of amorphous Zr-Ge alloys are also plotted for reference.

The value of θ_D, which is the other dominating parameter for T_c, is not determined in the present study. However, the data of the Young's modulus sound velocity may allow one to predict the compositional dependence of the θ_D values from the following equation based on the Debye approximation [28], even though the velocity was measured at ambient temperatures.

$$V_E = \omega_D\left[\frac{6\pi^2 N}{\Omega}\right]^{-1/3} = \frac{k_B\theta_D}{\hbar}\left[\frac{6\pi^2 N}{\Omega}\right]^{-1/3} \qquad (6)$$

Here ω_D is the Debye phonon frequency and N/Ω the number of atoms per unit volume. This equation clearly indicates that the increase in the Young's modulus sound velocity with increasing germanium content shown in Fig. 4 corresponds to the increases in the Debye phonon frequency and the Debye temperature. Accordingly, it is concluded that θ_D of the bcc Zr-Ge alloy increases with increasing germanium content. Nevertheless, as shown in Fig. 6, the increase in zerconium content results in a lowering of T_c. From the above results, it is concluded that the T_c values of Zr-Ge alloys in the metastable bcc

and amorphous phases are not primarily governed by the Debye temperature.

The Eliashberg equation by McMillan [25], which gives the accurate numerical solution of T_c, describes the relation between the electron-phonon coupling constant λ and the phonon frequency ω as follows:

$$\lambda = 2\int_0^\infty \alpha^2(\omega)F(\omega)\,d\omega/\omega \tag{7}$$

Here $F(\omega)$ is the phonon spectrum and $\alpha(\omega)$ the electron-phonon matrix element. Although the quantity $\alpha^2(\omega)F(\omega)$ is not known in the present study, one can infer by using the McMillan's factorization of λ [25].

$$\lambda = \frac{N(E_f)\langle I^2\rangle}{M\langle\omega^2\rangle} \tag{8}$$

where $\langle I^2\rangle$ is the average over the Fermi surface of the square of the electronic matrix element, M the average ionic mass and $\langle\omega^2\rangle$ an average of the square of the phonon frequency. The data of the Young's modulus sound velocity as a function of germanium shown in Fig. 4 indicate that the values of $\langle\omega^2\rangle$ increases with increasing germanium content, resulting in a decrease in λ, even though the values of $N(E_f)\langle I^2\rangle$ remain unknown for the Zr-Ge alloys. The change in λ with varying germanium content is consistent with the above-described correlation between T_c and λ.

3. Parameters characterizing the nonequilibrium bcc superconductor

In an extended GLAG theory for "dirty" superconductors [27], the GL coherence length $\xi_{GL}(0)$ at 0 K, the extrinsic GL parameter κ, the penetration depth λ_0 at 0 K and the electronic diffusivity D are expressed by the following relations and the values estimated from the expressions are also shown in Table 1.

$$\xi_{GL}(0) = 1.0\times10^{-6}(\rho_n\gamma T_c)^{-1/2} \tag{9}$$

$$\kappa = 7.49\times10^{3}\gamma^{1/2}\rho_n \tag{10}$$

$$\lambda_0 = 1.05\times10^{-2}(\rho_n/T_c)^{1/2} \tag{11}$$

$$D = \frac{4k_Bc}{e}\left[\frac{dH_{c2}}{dT}\right]^{-1}_{T_c} \tag{12}$$

As seen in the table, the κ, $\xi_{GL}(0)$ and λ_0 increase from 69 to 76, 7.2 to 7.7 nm and 695 to 817 nm, respectively, with increasing germanium content, while the D value decreases from 48.8 to 47.1 mm^2/s. The high values of κ, $\xi_{GL}(0)$ and λ_0 and the low value of D appear to

originate from a small value of the electron mean free path in the solid solution saturated with germanium containing a high density of internal defects, as evidenced by the high electrical resistivity ranging from 1.70 to 2.00 μΩm. Therefore, it is concluded that the present bcc Zr-Ge superconductors are typical type-II material characterized as extremely high degree of dirtiness, being similar to the amorphous superconductors. However, the degree of dirtiness significantly decreases upon the structural change from amorphous to bcc phases, suggesting that atomic configurations in the bcc alloys are in much less random state on the scale much smaller than $\xi_{GL}(0)$.

4. Comparison of the hardness, Young's modulus sound velocity and the superconducting characteristics between bcc and amorphous phases

As shown in the section 3, the structural change of the bcc to amorphous phase results in the drastic changes of hardness and Young's modulus sound velocity, while no apparent discontinuity at the bcc and amorphous phase boundaries is seen in the superconducting and electrical properties of T_c, ΔT_c, $-(dHc2/dT)_{Tc}$, ρ_n and $1/\rho_{R.T.}$ $(d\rho/dT)$ and in the fundamental parameters for superconductivity such as $N(E_f)(1+\lambda)$, $\xi_{GL}(0)$, κ, λ_0 and D. The marked difference of the composition dependence suggests that the hardness and Young's modulus sound velocity appear to be dominated by the long-range atomic configurations and hence are very sensitive to the structural change from the bcc to amorphous phase, whereas the other properties are closely related to the local atomic configurations on the scale of atomic distances. The monotonous variations of the properties in the vicinity of the bcc to amorphous phase suggest a great similarity of the atomic configurations on the localized scale of atomic distances between the bcc and amorphous phases. It is of vital interest to carry out the detailed investigation on the local atomic configuration in the bcc and the amorphous phases.

5. Summary and conclusions

A metastable bcc phase exhibiting superconductivity was found in melt-quenched Zr-Ge binary alloys. The formation range of the bcc phase was 9 to 12 at% Ge. Specimens were produced in the form of a continuous ribbon of about 1 mm wide and about 0.02 mm thick using a melt spinning apparatus in which the alloy was levitation melted. The bcc alloys are completely ductile and can be folded together without fracture. The hardness (H_V) and Young's modulus sound velocity (V_E) gradually increase with germanium content. The bcc alloys showed a sharp superconducting transition from high electrical re-

sistivities. With increasing germanium content, T_c decreased from 3.88 to 3.30 K, while the $-(dH_{c2}/dT)_{T_c}$ at T_c and ρ_n at 4.2 K increased from 1.79×10^6 to 1.86×10^6 Am^{-1} K^{-1} and 1.70 to 2.00 $\mu\Omega m$, respectively. A strong correlation among ρ_n, $1/\rho_{R.T.}(d\rho/dT)$, T_c and $-(dH_{c2}/dT)_{T_c}$ was found; with decreasing ρ_n or with increasing $1/\rho_{R.T.}(d\rho/dT)$, T_c increases and $-(dH_{c2}/dT)_{T_c}$ decreases. The existence of the correlation between T_c and ρ_n or $1/\rho_{R.T.}(d\rho/dT)$ was inferred to reflect on the strong correlation between λ and ρ_n or $1/\rho_{R.T.}(d\rho/dT)$. $N(E_f)(1+\lambda)$ was calculated from the experimentally measured values of ρ_n and $-(dH_{c2}/dT)_{T_c}$ by using the strong-coupling theories. The T_c versus $N(E_f)(1+\lambda)$ or V_E plot suggests that Tc is mainly governed by $N(E_f)$ or λ rather than θ_D. Further, the values of $\xi_{GL}(0)$, κ, and λ_0 were estimated to be about 7.5 nm, 69-76 and 695-817 nm, respectively, from the experimental values of $-(dH_{c2}/dT)_{T_c}$ and ρ_n by using the extended GLAG theory. It was therefore concluded that the metastable bcc alloys are typical "dirty" type-II superconductor.

Acknowledgements

The present authors would like to thank Dr. N. Toyota and Assistant Prof. T. Fukase in the Research Institute for Iron, Steel and Other Metals, Tohoku University for many suggestions on the interpretation of the results.

References

(1) W. L. Johnson, Rapidly Quenched Metals III, Vol. 2, ed. by B. Cantor, The Metals Society, London, 1978, p. 1.

(2) W. L. Johnson, J. Phys., C-8 (1980), 731.

(3) A. Inoue and T. Masumoto, Sci. Rep. Res. Inst. Tohoku University, A29 (1981), 305.

(4) N. Toyota, T. Fukase, A. Inoue, Y. Takahashi and T. Masumoto, Physica 107B (1981), 465.

(5) A. Inoue, Y. Takahashi, N. Toyota, T. Fukase and T. Masumoto, Proc. of the Fourth Intern. Conf. on Rapidly Quenched Metals, Vol. 2, ed. by T. Masumoto and K. Suzuki, The Japan Institute of Metals, Sendai, 1982, p. 1221.

(6) A. Inoue, Y. Takahashi, N. Toyota, T. Fukase and T. Masumoto, J. Mater. Sci., 17 (1982), 2218.

(7) T. Masumoto, A. Inoue, S. Sakai, H. M. Kimura and A. Hoshi, Trans. Japan Inst. Metals, 21 (1980), 115.

(8) A. Inoue, H. M. Kimura, T. Masumoto, C. Suryanarayana and

A. Hoshi, J. Appl. Phys., 51 (1980), 5475.
(9) Metals Databook, The Japan Institute of Metals, Maruzen, Tokyo, 1974, p. 46.
(10) A. Inoue, Y. Takahashi, N. Toyota, T. Fukase and T. Masumoto, J. Mater. Sci., in press.
(11) A. Inoue, H. S. Chen, J. T. Krause and T. Masumoto, to be published.
(12) J. H. Mooij, Phys. Stat. Sol. (a), 17 (1973), 521.
(13) H. J. Güntherodt and H. U. Künzi, Metallic Glasses, American Society for Metals, New York, 1978, p. 247.
(14) S. R. Nagel, Advance in Chemical Physics, ed. by I. Prigogine and S. A. Rice, John Wiley and Sons, New York, 1982, 51, p. 227.
(15) R. W. Roberts, Properties of Selected Superconductive Materials, NBS Technical Note 983, U.S. Department of Commerce, Washington, 1978, p. 12.
(16) K. Samwer and H. V. Löhneysen, Phys. Rev. B, 26 (1982), 107.
(17) L. R. Testardi, IEEE Trans. on Magnetics, MAG-11 (1975), 197.
(18) J. M. Poate, L. R. Testardi, A. R. Storm and Augustyniak, Phys. Rev. Lett., 35 (1975), 1290.
(19) H. Lutz, H. Weismann, O. F. Kammerer and M. Strongin, Phys. Rev. Lett., 36 (1976), 1576.
(20) A. Inoue, T. Masumoto and H. S. Chen, J. Phys. F: Metals Phys., to be submitted.
(21) A. Inoue, Y. Takahashi, N. Toyota, T. Fukase and T. Masumoto, J. Mater. Sci., in press.
(22) A. Inoue, Y. Takahashi, N. Toyota, T. Fukase and T. Masumoto, Trans. Japan Inst. Metals, 23 (1982), No. 11.
(23) A. Inoue, Y. Takahashi, K. Aoki, S. Sakai and T. Masumoto, Proc. of the Fourth Intern. Conf. on Rapidly Quenched Metals, Vol. 2, ed. by T. Masumoto and K. Suzuki, The Japan Institute of Metals, Sendai, 1982, p. 1245.
(24) J. J. Hopfield, Superconductivity in d- and f-band Metals, ed. by D. H. Douglass, AIP, New York (1972), p. 358.
(25) W. L. McMillan, Phys. Rev., 167 (1968), 331.
(26) N. F. Mott and H. Jones, The Theory of the Properties of Metals and Alloys, Dover, New York, 1936, p. 97.
(27) For example, T. R. Orlando, E. J. Mcniff, Jr., S. Forner and M. R. Beasley, Phys. Rev. B, 19 (1979), 4545.
(28) T. Otsuka, Ferroelectrics and Superconductor, ed. by The Japan Institute of Metals, Sendai, 1973, p. 131.